

Suzaku observation of Galactic supernova remnant CTB 37A (G348.5+0.1)

A. Sezer,^{1,2*} F. Gök,³ M. Hudaverdi¹ and E.N. Ercan^{2*†}

¹*TÜBİTAK Space Technologies Research Institute, ODTU Campus, Ankara, 06531, Turkey*

²*Boğaziçi University, Faculty of Art and Sciences, Department of Physics, İstanbul, 34342, Turkey*

³*Akdeniz University, Faculty of Sciences, Department of Physics, Antalya, 07058, Turkey*

ABSTRACT

We present here the results of the observation of CTB 37A obtained with the X-ray Imaging Spectrometer onboard the *Suzaku* satellite. The X-ray spectrum of CTB 37A is well fitted by two components, a single-temperature ionization equilibrium component (VMEKAL) with solar abundances, an electron temperature of $kT_e \sim 0.6$ keV, absorbing column density of $N_H \sim 3 \times 10^{22} \text{ cm}^{-2}$ and a power-law component with photon index of $\Gamma \sim 1.6$. The X-ray spectrum of CTB 37A is characterized by clearly detected K-shell emission lines of Mg, Si, S, and Ar. The plasma with solar abundances supports the idea that the X-ray emission originates from the shocked interstellar material. The ambient gas density, and age of the remnant are estimated to be $\sim 1 f^{-1/2} \text{ cm}^{-3}$ and $\sim 3 \times 10^4 f^{1/2} \text{ yr}$, respectively. The center-filling X-ray emission surrounded by a shell-like radio structure and other X-ray properties indicate that this remnant would be a new member of mixed-morphology supernova remnant class.

Key words: ISM: supernova remnants—ISM:individual(CTB 37A)—X-rays:ISM

1 INTRODUCTION

CTB 37A (also called G348.5+0.1, RA(2000) = $17^{\text{h}}14^{\text{m}}06^{\text{s}}$, Dec. (2000) = $-38^{\circ}32'$) was discovered by Clark, Caswell & Green (1975) in the radio band and has a shell-type morphology with an angular size of 15 arcmin. From Very Large Array observations at wavelengths of 6, 20, and 90 cm, Kassim, Baum & Weiler (1991) reported that this supernova remnant (SNR) is expanding in an inhomogeneous region, and is part of a complex composed of three SNRs: CTB 37A, G348.7+0.3 (also called CTB 37B), and G348.5-0.0. From the *ASCA* Galactic plane survey data of G348.5+0.1, Yamauchi et al. (2008) found that the X-ray spectra of the SNR was heavily absorbed by interstellar matter with $N_H \sim 2 \times 10^{22} \text{ cm}^{-2}$ and the size of X-ray emission was comparable to its radio structure. Frail et al. (1996) detected OH masers with velocities at about 20 and 60 km s^{-1} , in the direction of CTB 37A at 1720 MHz. Reynoso & Mangum (2000) surveyed the environment of this remnant with associated

OH 1720 MHz masers in the CO J=1-0 transition with the 12 Meter Telescope of the NRAO. They reported that a number of molecular clouds are interacting with the SNR shock fronts. Aharonian et al. (2008) using *Chandra* and *XMM-Newton* data showed the presence of thermal X-rays from the Northeast part, an extended non-thermal X-ray source, CXOU J171419.8-383023 in the Northwest part and a γ -ray source, HESS J1714-385, coincident with the remnant. They found a high absorbing column density of $N_H \sim 3 \times 10^{22} \text{ cm}^{-2}$. They claimed that the observed X-ray morphology was a result of interaction with the inhomogeneous medium surrounding the remnant and this inhomogeneity was also responsible for the break-out radio morphology. Castro & Slane (2010) using observations with the Fermi-LAT, have revealed γ -ray emission from this SNR; the spectrum of the source coincident with CTB 37A was fitted by a power-law (PL) model with an exponential cutoff at energy $E_{\text{cut}}=4.2$ GeV. Considering the lack of evidence for contribution by a pulsar and the presence of maser emission for the remnant they proposed that γ -rays result from SNR-molecular clouds interactions.

* E-mail: aytap.sezer@uzay.tubitak.gov.tr (AS); gok@akdeniz.edu.tr (FG); murat.hudaverdi@uzay.tubitak.gov.tr (MH); ercan@boun.edu.tr (ENE).

† This file has been amended to highlight the proper use of $\LaTeX 2_{\epsilon}$ code with the class file. These changes are for illustrative purposes and do not reflect the original paper by A. Sezer.

The distance to the CTB 37A has been estimated from 21 cm absorption measurement to be in between 6.7-13.7 kpc by Caswell et al. (1975). From velocity measurements of molecular clouds associated with the remnant, Reynoso & Mangum (2000) adopted a distance of 11.3 kpc.

So we will use $d=11.3$ kpc for our calculations throughout this work.

The location of CTB 37A containing OH maser sources (Frail et al. 1996), 1FGL J1714.5-3830 (Castro & Slane 2010), X-ray source CXOU J171419.8-383023, and HESS J1714-385 (Aharonian et al. 2008), as well as two additional SNRs (G348.5-0.0 and G348.7+0.3) make this SNR interesting and important. In addition, its morphology implies a similarity to the recently proposed group of mixed-morphology (MM) SNRs, increasing its importance. High quality imaging and spectra obtained from the data provided by X-ray observatory *Suzaku* are used to produce the results in this work.

The organization of this paper is as follows: we describe the *Suzaku* X-ray observation of CTB 37A, including details of data reduction in Section 2. The image and spectral analysis are given in Sections 3 and 4, respectively. Finally, considering its morphology and investigating radial variation of the electron temperature, we discuss the implications of MM class, the nature of thermal and non-thermal components of CTB 37A in Section 5.

2 OBSERVATION AND DATA REDUCTION

Suzaku (Mitsuda et al. 2007) is the fifth Japanese X-ray astronomy satellite launched on 2005 July 10. *Suzaku* has observed CTB 37A on 2010 February 20. The observation ID and exposure time are 504097010 and 53.8 ks, respectively. The X-ray Imaging spectrometer (XIS; Koyama et al. (2007)) consists of four sets of X-ray CCD camera system (XIS0, 1, 2 and 3). XIS0, 2, and 3 have front-illuminated (FI) sensor and provide coverage over the energy range 0.4–12 keV, while XIS1 has a back-illuminated (BI) sensor providing greater sensitivity at lower energies (0.2–12 keV). The XIS has a field of view (FOV) of 17.8×17.8 arcmin² (1024×1024 pixels). Each XIS CCD has an ⁵⁵Fe calibration source, which can be used to calibrate the gain and test the spectral resolution of data taken using this instrument. The XIS2 sensor was available only until 2006, therefore, we use data of XIS0, XIS1, XIS3.

Reduction and analysis of the data were performed following the standard procedure using the HEADAS software package of version 6.5 and spectral fitting was performed with XSPEC version 11.3.2 (Arnaud 1996). The XIS was operated in the normal full-frame clocking mode, with the standard 3×3 and 5×5 editing mode. We generated XIS response matrices using the XISRMFGN software, which takes into account the time-variation of the energy response. As for generating ancillary response files (ARFs), we used XIS-SIMARFGN (Ishisaki et al. 2007). The latest version of the relevant *Suzaku* CALDB files were also used.

3 IMAGE ANALYSIS

Figure 1 shows XIS1 image in 0.3–10 keV energy band. We extracted the spectrum from the brightest region represented with the outermost solid circle centered at $RA(2000) = 17^{\text{h}}14^{\text{m}}30^{\text{s}}$, $Dec. (2000) = -38^{\circ}32'07''$ with a radius of 5.5 arcmin. To derive the radial variation of the electron temperature kT_e , we take four apertures with sizes

of 0–1.5, 1.5–2.5, 2.5–3.5, 3.5–4.5 arcmin. The extended non-thermal X-ray source (CXOU J171419.8-383023) is excluded from spectral analysis as shown in Fig. 1. The dashed black circle centered at $(RA(2000) = 17^{\text{h}}14^{\text{m}}19^{\text{s}}$, $Dec. (2000) = -38^{\circ}24'36''$ with radius 1.7 arcmin) represents the background region. The lower left corner in the FOV that contains calibration source emission is also extracted.

Figure 2 shows the XIS0 image in 0.3–10 keV energy band, which is overlaid with the radio image obtained at 843 MHz by Whiteoak & Green (1996) for comparison. Dark crosses indicate the direction of the detected OH (1720 MHz) maser emission at velocities ~ -65 km s⁻¹ associated with CTB 37A, and the white crosses show the positions of maser emission at velocities ~ -22 km s⁻¹ (Frail et al. 1996). The diamond indicates the position of CXOU J171419.8-383023 and the circle represents the location of HESS J1714-385 (Aharonian et al. 2008).

4 SPECTRAL ANALYSIS

XIS spectra were extracted using XSELECT version 2.4a from all the XISs with a circular extraction region of radius 5.5 arcmin and are grouped with a minimum of 50 counts bin⁻¹. We fit the spectra with a collisional ionization equilibrium (CIE) model with variable abundances (XSPEC model “VMEKAL”; Mewe Gronenschild & van den Oord (1985); Mewe, Lemen & van den Oord (1986); Liedahl, Osterheld & Goldstein (1995)) modified by interstellar absorption (wabs in XSPEC, Morrison & McCammon (1983)). The parameters of the absorbing column density (N_{H}) and electron temperature (kT_e) are set free while all elements were fixed at solar abundances (Anders & Grevesse 1989). The best-fitting reduced $\chi^2/\text{d.o.f.}$ for this model is $2222.5/832 = 2.67$. To find out if there was any contribution from non-thermal emission we added a PL component (VMEKAL+PL) yielding a better reduced χ^2 of $935.5/830 = 1.13$. Then, Mg, Si, S and Ar lines in the spectrum were set free, while the rest were fixed at their solar values, we found insignificant improvement in χ^2 value ($891.6/826 = 1.08$). Therefore, we decided to fix the abundances of Mg, Si, S, and Ar at their solar values. In Table 1, we present the best-fitting parameters and the statistics obtained with an absorbed VMEKAL+PL with corresponding errors at 90 per cent confidence level (2.7σ). Figure 3 shows the spectra of the XIS0, XIS1, and XIS3 simultaneously, in the energy range of 0.3–10 keV that is taken from the region shown by the solid dark circle (the outermost) presented in Fig. 1. On the other hand, we performed annular spectral analysis for four regions shown by the circles in Fig. 1 to be able to derive the radial temperature variations of CTB 37A. The annular regions are spaced by 1 arcmin from the innermost circle with radius $r=1.5$ arcmin. VMEKAL+PL spectral model were also fitted to each annulus, while fitting them we kept the absorbing column density N_{H} at its best-fitting value for the entire remnant. Figure 4 shows the electron temperature variations with respect to the radius.

Table 1. Best-fitting parameters and χ^2 values of the spectral fitting in the full energy band (0.3–10 keV) with an absorbed VMEKAL+PL model with corresponding errors at 90 per cent confidence level (2.7 σ).

Component	Parameters	VMEKAL+PL
Wabs	$N_{\text{H}}(\times 10^{22} \text{cm}^{-2})$	2.9 ± 0.1
VMEKAL	$kT_{\text{e}}(\text{keV})$	0.63 ± 0.02
Abundance ^a	Mg	(1)
	Si	(1)
	S	(1)
	Ar	(1)
	VEM ^b	72.3 ± 2.1
	Flux ^c	1.36 ± 0.03
PL	Photon Index	1.6 ± 0.1
	norm($\times 10^{-2}$ photons $\text{cm}^{-2} \text{s}^{-1}$)	1.9 ± 0.2
	Flux ^d	1.5 ± 0.1
	$\chi^2/\text{d.o.f.}$	935.6/830=1.13

^a (1) indicates that the elemental abundance is fixed at solar (Anders & Grevesse 1989).

^b Volume emission measure $\text{VEM} = \int n_{\text{e}} n_{\text{H}} dV$ in the unit of 10^{58}cm^{-3} , where n_{e} and n_{H} are number densities of electrons and protons, respectively, and V is the X-ray emitting volume.

^c Unabsorbed flux in the 0.3 – 10 keV energy band in the unit of $10^{-9} \text{erg s}^{-1} \text{cm}^{-2}$.

^d Total unabsorbed flux of the sum of the VMEKAL and PL components in the 0.3 – 10 keV energy band in the unit of $10^{-9} \text{erg s}^{-1} \text{cm}^{-2}$.

5 DISCUSSION AND CONCLUSIONS

In this work, we provide a description of the X-ray emission of CTB 37A based on *Suzaku* archival data. We obtained a clear image and high quality spectra of diffuse X-ray emission. We have examined the thermal and non-thermal emissions coming from the remnant. The X-ray spectrum of CTB 37A is characterized by thermal emission dominated by K-shell emission lines of Mg, Si, S, and Ar which are clearly detected.

As seen from Fig. 2, the radio emission of CTB 37A comprises a partial shell towards the north and east and an extended outbreak to the south, while the X-ray emission has a deformation along the southwest limb, where the morphology appears indented. The reason for such a deformation may be due to the inhomogeneous medium along this specific region and this may well be supported by the fact that remnant is close to the Galactic plane and several OH masers at 1720 MHz are detected towards CTB 37A (Frail et al. 1996) (shown by crosses). It may also be relevant that γ -ray emission thought to be associated with the interaction between CTB 37A and dense surrounding material that has been detected with the *Fermi* LAT (Castro & Slane 2010).

5.1 Implications for mixed-morphology

SNRs were originally divided into shell-like, Crab-like (plerionic), and composite (shell-like containing plerions) remnants (Seward 1985) according to their X-ray morphology. Recently, an additional MM class (also called thermal composite) appeared, which are center-filled in X-rays and shell-like at radio wavelengths (Seward 1990; Jones et al. 1998; Rho & Petre 1998). As seen from Fig. 2, CTB 37A has a shell-like morphology in the radio band while centrally-filled in X-ray band, in this regard, our first impression is CTB 37A seems to be a MM SNR. Examples of well-known

MM SNRs include W28 (Rho & Borkowski 2002), G290.1-0.8 (Slane et al. 2002), and IC 443 (Kawasaki et al. 2002). Lazendic & Slane (2006) reported important results about this class by compiling a list of 26 MM SNRs.

The X-ray characteristics of MM remnants have been defined by Rho & Petre (1998) as follows: (1) The radial temperature distribution is relatively flat; (2) The X-ray emission arises primarily from shocked interstellar material, and not from ejecta; (3) The remnants are typically located close to molecular clouds or very dense regions; and (4) The dominant X-ray emission is thermal in nature. Subsequent studies indicated that MM SNRs had a complex plasma structure with multiple components (e.g. Rho & Borkowski (2002)) and enhanced abundances (e.g. Yamauchi et al. (1999); Slane et al. (2002)), and they have evolved over $\sim 10^4$ yr, which means that the plasma is in CIE or an overionization condition (Kawasaki et al. 2005). As can be seen from Fig. 4, the annular analysis of CTB 37A may well be indicating a very small scale radial variation in its temperature between the selected regions. The best-fitting metal abundances are found to be solar in general, confirming the absence of ejecta contamination in selected regions. It may support the idea that the X-ray emission originates from the shocked interstellar material. The plasma of CTB 37A is in a collisional ionization equilibrium condition and is located in a region with density variation, possibly associated with molecular clouds. The plasma has thermal and non-thermal emission, but the emission is dominated by thermal component (~ 90 per cent of the total X-ray flux). These X-ray properties of CTB 37A exemplify the typical characteristic of MM SNRs as defined by (Rho & Petre 1998).

There are a few models that can produce centrally enhanced X-ray emission such as evaporation of clouds left relatively unspoiled after the passage of the SNR blast wave (e.g. White & Long (1991)) and “fossil” thermal radiation

that is detectable as thermal X-rays from the hotter interior as the shell of an expanding SNR cools below $\sim 10^6$ K and becomes invisible due to interstellar absorption (e.g. Seward (1985)), as the SNR evolves, the temperature and density of the hot interior plasma gradually become uniform through thermal conduction (e.g. Cox et al. (1999)) or evolution in a medium with a density gradient viewed along the line of sight (Petruk 2001). The evaporation model requires dense clouds, the thermal conduction model requires a relatively high density ambient medium. CTB 37A is located in a region of greatly varying density, with OH maser sources indicating interaction with molecular clouds. In this regard, the center-filled X-ray morphology of CTB 37A is consistent with evaporating clouds model. The radial temperature variation in the plasma of CTB 37A ($kT_e \sim 0.6-0.8$ keV) is consistent with other MM SNRs such as W44 (Rho et al. 1994; Shelton, Kuntz & Petre 2004), 3C391 (Rho & Petre 1996; Chen et al. 2004) and HB21 (Pannuti et al. 2010). Very small temperature variation in the plasma of CTB 37A as shown Fig. 4 can be explained by both evaporation and thermal conduction models. Future deep X-ray observations and detailed spectral analysis of this remnant would give more detailed information to compare with theoretical models that produce MM SNRs.

5.2 Thermal component

The X-ray emission of CTB 37A is dominated by thermal emission that can be best described by an absorbed CIE plasma model (VMEKAL) with an absorbing column density of $N_H \sim 3 \times 10^{22} \text{ cm}^{-2}$, an electron temperature of $kT_e \sim 0.6$ keV, and solar abundances of Mg, Si, S, and Ar, which indicate a shocked interstellar/circumstellar material origin.

For full ionization equilibrium, the ionization timescale, $\tau = n_e t$, is required to be $\geq 10^{12} \text{ cm}^{-3} \text{ s}$, where t is the plasma age or the time since the gas was shock-heated (Masai 1984). To determine the age of the remnant, n_e should be estimated from the emission measure, $n_e n_H V$, which is related to the normalization of the VMEKAL model according to the equation, $\text{norm} = n_e n_H V / (4\pi d^2 10^{14})$, where V is the X-ray emitting volume, n_H is the volume density of hydrogen and d is the distance. For simplicity, we assumed the emitting region to be a sphere of radius 5.5 arcmin. Considering the possibility that less than the entire volume is filled, we write the volume $V = V_s f$, where V_s is the full spherical volume, f is the filling factor. We then carry the f factor through our calculations to show the explicit dependence of each derived quantity on this factor. Knowing that the SNR is at a distance of 11.3 kpc and $n_e = 1.2 n_H$, we estimated the emission volume to be $V \sim 6.7 \times 10^{59} f \text{ cm}^3$. Consequently, we find an ambient gas density of $\sim 1 f^{-1/2} \text{ cm}^{-3}$ and age of $\sim 3 \times 10^4 f^{1/2} \text{ yr}$ (assuming $n_e t \sim 1 \times 10^{12} \text{ cm}^{-3} \text{ s}$), implying that CTB 37A is a middle-aged SNR. Finally, we calculated total mass of the X-ray emitting plasma, M_x , by $M_x = m_H n_e V \sim 530 f^{1/2} M_\odot$, where m_H is mass of a hydrogen atom, $\mu = 0.604$ is the mean atomic weight.

5.3 Power-law component

The Suzaku X-ray spectral data of CTB 37A is well fitted with a thermal component and an additional hard compo-

nent. There could be a few reasons for the hard X-ray emission: (i) an association with a classical young pulsar, (ii) a contribution from an extended non-thermal X-ray source (CXOU J171419.8-383023), (iii) overionization of the plasma which produces excess hard emission as has been the case for IC443 (Yamaguchi et al. 2009). The hard component is well fitted by a PL model with a photon index value of ~ 1.6 . This value is consistent with that of classical young pulsar value ranging in between 1.1 and 1.7 (Chakrabarty et al. 2001). However, there is no pulsar reported that is associated with this remnant. In the Northwest region of the CTB 37A, an extended non-thermal X-ray source (CXOU J171419.8-383023) is reported (RA(2000) = $17^{\text{h}}14^{\text{m}}20^{\text{s}}$, Dec. (2000) = $-38^{\circ}30'20''$) by Aharonian et al. (2008). In their work, a non-thermal emission from the source with a spectral index of ~ 1.32 is found which is lower (harder) than our best-fitting value of ~ 1.6 . Although we excluded CXOU J171419.8-383023 (with radius 2.1 arcmin) from our spectra during our spectral analysis, our fits required a non-thermal component. To investigate this, we performed spectral analysis also for individual regions by selecting small rectangular regions that are being further away from the known extended non-thermal source. The non-thermal flux is found to be stronger for the selected small regions nearby the source compared to the ones further away. We have obtained an unabsorbed flux value of $F_x \sim 1.4 \times 10^{-9} \text{ erg s}^{-1} \text{ cm}^{-2}$ for the non-thermal extended source in the 0.3–10 keV energy range. When we compare it with the unabsorbed flux value ($F_x \sim 0.14 \times 10^{-9} \text{ erg s}^{-1} \text{ cm}^{-2}$) of PL component of best-fitting, we find a factor of ten difference between them. This difference indicates that the extended source is most likely the origin of the PL component and emission scattered from the source into the field of the rest of the remnant by a broad point spread function of the *Suzaku* mirrors.

The spectral studies of CTB 37A indicate that the plasma is best described by a thermal component in CIE condition with solar elemental abundances and a non-thermal component with a photon index of ~ 1.6 . Thermal emission possibly originates from the shocked interstellar material with ambient gas density of $\sim 1 f^{-1/2} \text{ cm}^{-3}$. The best spectral fits require an ionization timescale of $\tau \geq 10^{12} \text{ cm}^{-3} \text{ s}$, implying an age of $\sim 3 \times 10^4 f^{1/2} \text{ yr}$. The origin of the power-law component is more likely the effect of the contribution from the extended source (CXOU J171419.8-383023) located in the Northwest part of the remnant. CTB 37A is most likely a new member of mixed-morphology SNR.

ACKNOWLEDGMENTS

We thank Dr. Patrick Slane for his valuable comments and suggestions which helped to improve the overall quality of the manuscript. AS is supported by TÜBİTAK Post-Doctoral Fellowship. This work is supported by the Akdeniz University Scientific Research Project Management and by TÜBİTAK under project codes 108T226 and 109T092. The authors also acknowledge the support by Boğaziçi University Research Foundation under 2010-Scientific Research Project Support (BAP) project no:5052.

REFERENCES

60, 1143

- Aharonian et al., 2008, *A&A*, 490, 685
- Anders E., Grevesse N., 1989, *Geochimica Cosmochimica Acta*, 53, 197
- Arnaud K. A., 1996, in Jacoby G., Barnes J., eds, *ASP Conf. Ser. Vol.101, Astronomical Data Analysis Software and Systems V*. Astron. Soc. Pac., San Francisco, p. 17
- Castro D., Slane P., 2010, *ApJ*, 717, 372
- Caswell J. L., Murray J. D., Roger R. S., Cole D. J., Cooke D. J., 1975, *A&A*, 45, 239
- Chakrabarty D., Pivovarov M. J., Hernquist L.E., Heyl J. S., Narayan R., 2001, *ApJ*, 548, 800
- Chen Y., Su Y., Slane P. O., Wang Q. D., 2004, *ApJ*, 616, 885
- Chevalier R. A., 1999, *ApJ*, 511, 798
- Clark D. H., Caswell J. L., Green A. J., 1975, *Australian Journal of Physics, Astrophysical Supplement*, 37, 1
- Cox D. P., Shelton R. L., Maciejewski W., Smith R. K., Plewa T., Pawl A., Różycka M., 1999, *ApJ*, 524, 179
- Frail D. A., Goss W. M., Reynoso E. M., Giacani E. B., Green A. J., Otrupcek R., 1996, *AJ*, 111, 1651
- Ishisaki Y. et al., 2007, *PASJ*, 59, 113
- Jones T. W. et al., 1998, *PASP*, 110, 125
- Kassim N.E., Baum S.A., Weiler K.W., 1991, *ApJ*, 374, 212
- Kawasaki M. T., Ozaki M., Nagase F., Masai K., Ishida M., Petre R., 2002, *ApJ*, 572, 897
- Kawasaki M., Ozaki M., Nagase F., Inoue H., Petre R., 2005, *ApJ*, 631, 935
- Koyama K. et al., 2007, *PASJ*, 59, 23
- Lazendic J. S., Slane P. O., 2006, *ApJ*, 647, 350
- Liedahl D. A., Osterheld A. L., Goldstein W. H., 1995, *ApJ*, 438, L115
- Masai K., 1984, *Ap&SS*, 98, 367
- Mewe R., Gronenschild E. H. B.M., van den Oord G. H. J., 1985, *A&AS*, 62, 197
- Mewe R., Lemen J. R., van den Oord G. H. J., 1986, *A&AS*, 65, 511
- Mitsuda K. et al., 2007, *PASJ*, 59, 1
- Morrison R., McCammon D., 1983, *ApJ*, 270, 119
- Pannuti T. G., Rho J., Borkowski K. J., Cameron P.B., 2010, *AJ*, 140, 1787
- Petruk O., 2001, *A&A*, 371, 267
- Reynoso E.M., Mangum J.G., 2000, *ApJ*, 545, 874
- Rho J., Petre R., Schlegel E. M., Hester J.J., 1994, *ApJ*, 430, 757
- Rho J., Petre R., 1996, *ApJ*, 467, 698
- Rho J., Petre R., 1998, *ApJ*, 503, L167
- Rho J., Borkowski K. J., 2002, *ApJ*, 575, 201
- Seward F. D., 1985, *Comments Astrophys.* XI, 1, 15
- Seward F. D., 1990, *ApJS*, 73, 781
- Shelton R. L., Kuntz K. D., Petre R., 2004, *ApJ*, 611, 906
- Slane P., Smith R. K., Hughes J. P., Petre R., 2002, *ApJ*, 564, 284
- White R. L., Long K. S., 1991, *ApJ*, 373, 543
- Whiteoak J.B.Z., Green A.J., 1996, *A&AS*, 118, 329
- Yamaguchi H., Ozawa M., Koyama K., Masai K., Hiraga J.S., Ozaki M., Yonetoku D., 2009, *ApJ*, 705, L6
- Yamauchi S., Koyama K., Tomida H., Yokogawa J., Tamura K., 1999, *PASJ*, 51, 13
- Yamauchi S., Ueno M., Koyama K., Bamba A., 2008, *PASJ*,

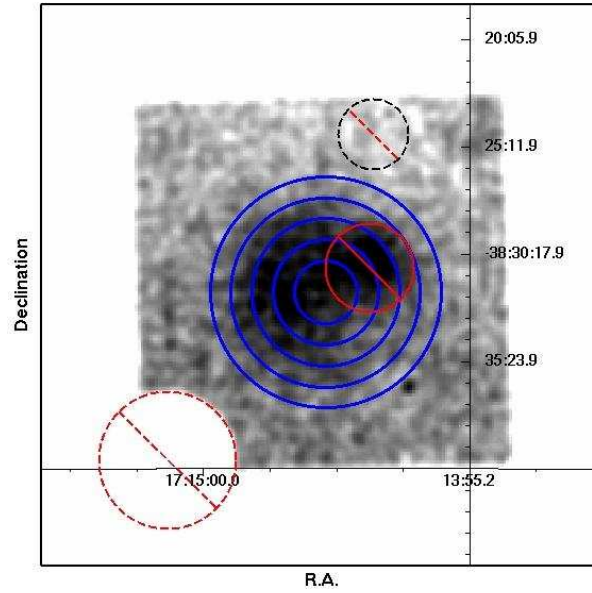


Figure 1. *Suzaku* XIS1 image of CTB 37A in the 0.3–10 keV energy band. The spectral integration regions for the source (annular apertures) and the background are indicated with the solid dark and dashed black circles, respectively. The X-ray source (CXOU J171419.8-383023) is extracted from the spectral analysis as shown in the figure. The corner of the CCD chip illuminated by ^{55}Fe calibration source is excluded from the image. The coordinates (RA and Dec) are referred to epoch J2000.

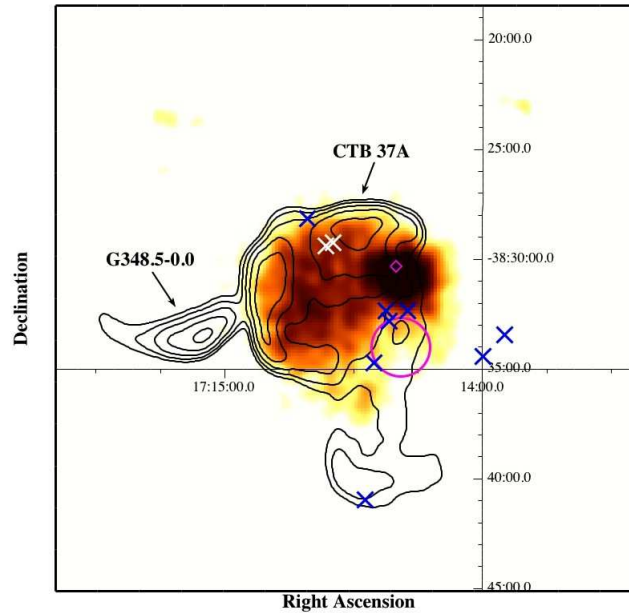


Figure 2. CTB 37A is displayed in 0.3–10 keV energy band X-ray data obtained from *Suzaku* XIS0 detector. The image is overlaid by 843 MHz radio isocontours logarithmically scaled (0.23, 0.36, 0.57, 0.90, 1.42, 2.23 and 3.51 mJy/Beam). Radio emission clearly shows 2 radio SNRs, CTB 37A and G348.5-0.0. X-ray data is smoothed with 3 pixel Gaussian in order to highlight the structure. The colour-coding shows the brightness levels from 1.3 counts/pix to 13.36 counts/pix in logarithmic scale from bright to dark. The masers from the field are indicated with dark and white crosses at velocities $\sim -65 \text{ km s}^{-1}$ and $\sim -22 \text{ km s}^{-1}$, respectively. The diamond shows the extended non-thermal X-ray source CXOUJ 171419.8-383023. The location of HESS J1714-385 is represented with the circle, in which the positional error is specified with the radius of 1.2 arcmin. The coordinates (RA and Dec) are referred to epoch J2000.

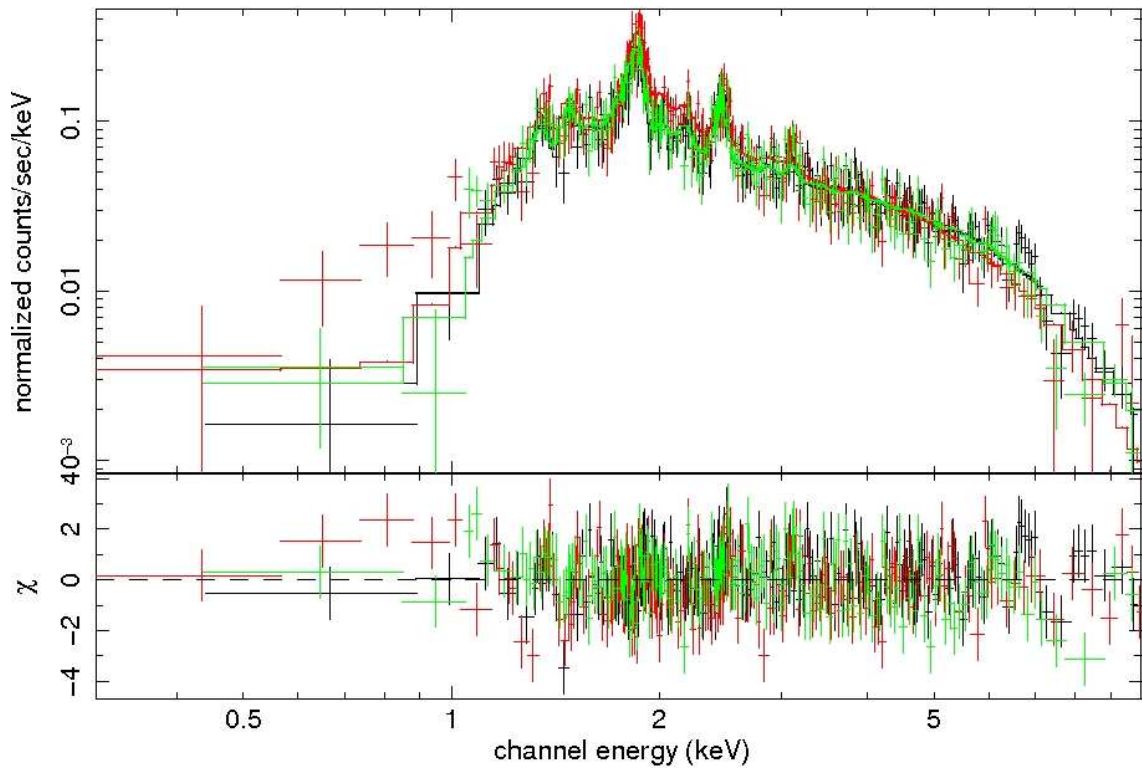


Figure 3. Background-subtracted XIS (XIS1, XIS0 and XIS3) spectra of CTB 37A in 0.3–10 keV energy band fitted with an absorbed VMEKAL and PL model. The bottom panel is the residuals from the best-fitting model.

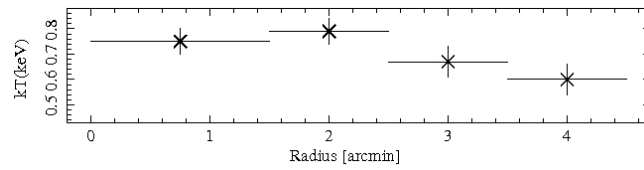


Figure 4. The radial variation of the electron temperature of CTB 37A.